

Directivity Enhancement of Movable Antenna Arrays with Mutual Coupling

Wei Xu, *Graduate Student Member, IEEE*, Lipeng Zhu, *Senior Member, IEEE*, Wenyan Ma, *Graduate Student Member, IEEE*, An Liu, *Senior Member, IEEE*, and Rui Zhang, *Fellow, IEEE*

Abstract—In conventional antenna arrays, mutual coupling between antenna elements is often regarded as detrimental. However, under specific conditions, it can be harnessed to enhance the far-field directivity (i.e., beamforming gain). Theoretically, the directivity of an N -antenna superdirective array over the endfire direction can reach N^2 , significantly exceeding the directivity of a traditional uncoupled array which is N over all directions. This paper investigates the potential of mutual coupling effects in movable antenna (MA) arrays for directivity enhancement. A low-complexity algorithm called Greedy Search and Gradient Descent (GS-GD) is proposed to optimize the antenna positions for maximizing the array directivity over any given direction, where the antenna positions are first selected sequentially from discrete grid points and then continuously refined through gradient descent (GD) optimization. Numerical results demonstrate that the optimized MA array design by exploiting the antenna coupling achieves significant directivity gains compared to the conventional uniform linear array (ULA) without antenna coupling over all directions. Additionally, the proposed GS-GD algorithm is shown to approach the global optimum closely in most directions.

Index Terms—movable antenna (MA) array, mutual coupling, directivity, antenna position optimization.

I. INTRODUCTION

In recent years, multiple-input multiple-output (MIMO) technology has achieved remarkable success in wireless communication systems. By increasing the number of antennas, MIMO systems can enhance both beamforming and multiplexing gains, thereby significantly improving the achievable transmission rate. However, the physical size constraints of modern devices and/or infrastructures necessitate placing multiple antennas in close proximity, which inevitably leads to mutual coupling between antenna elements. Such mutual coupling distorts the signals and is usually regarded to be harmful to the system performance. Numerous studies aim to eliminate or mitigate mutual coupling based on physical isolation or signal processing techniques [1], [2]. Meanwhile, several recent works indicate that coupled arrays can improve the far-field directivity (i.e., beamforming/array gain in a line-of-sight scenario) by appropriately adjusting the effective radiation pattern [3], [4]. For example, for an N -antenna uniform linear array (ULA) with the inter-antenna spacing approaching zero (i.e., superdirective array [5]), the directivity over the endfire direction (i.e., the direction aligned with the linear array) can reach N^2 [3], [4]. In comparison, the directivity for an uncoupled ULA with half-wavelength spacing (i.e.,

ULAH) is always N over all directions. This phenomenon of coupled arrays is known as superdirectivity. Although superdirective arrays can achieve higher beamforming gains over the endfire direction, they suffer from substantially lower gain over other directions compared to uncoupled arrays. In other words, the directivity of an antenna array depends on the array geometry (i.e., antennas' positions) and its maximum value varies with the wave direction. Thus, the maximum directivity over all wave directions cannot be simultaneously achieved by any array with fixed-position antennas (FPAs). Recently, movable antenna (MA) array has been proposed to enhance wireless communication performance by exploiting the degrees of freedom (DoFs) in antenna position optimization [6], [7], [8]. Joint antenna position and rotation design is also considered in six-dimensional MA (6DMA) systems [9], [10]. However, most existing studies assume that no mutual coupling exists between MA elements by constraining the inter-antenna spacing being greater than half-wavelength [11]. While prior works have demonstrated through simulations that mutual coupling can enhance the performance of dipole MA or reconfigurable intelligent surface (RIS) systems [12], [13], to the best of our knowledge, a theoretical framework quantifying the fundamental beamforming gain of general MA systems remains absent. To this end, this paper takes an isotropic MA array as a case study to establish a systematic framework for harnessing mutual coupling to enhance MA array directivity. In this paper, we first provide the expression of the directivity to illustrate the increased beamforming gain obtained by the coupled MA array. Then, for any given direction, we formulate an optimization problem to maximize the directivity by designing the antenna positions within the movable region. To solve the optimization problem, we propose a low-complexity Greedy Search and Gradient Descent (GS-GD) algorithm, where the antenna positions are first selected sequentially from discrete grid points and then continuously refined through gradient descent (GD) optimization. Extensive simulation results demonstrate the directivity gain of the coupled MA array and the efficiency of the proposed GS-GD algorithm.

Notations: $\mathbf{0}_N$ and \mathbf{I}_N refer to an all-zero column vector of dimension N and an $N \times N$ identity matrix, respectively. $\overline{(\cdot)}$, $(\cdot)^T$, $(\cdot)^H$, $(\cdot)^{-1}$ and $\Re(\cdot)$ denote conjugate, transpose, conjugate transpose, inverse and real part, respectively. \mathbb{R} and \mathbb{C} refer to the sets of real numbers and complex numbers, respectively. $|a|$ and $\|a\|_2$ denote the amplitude of scalar a and the 2-norm of vector \mathbf{a} , respectively. a_n and A_{mn} refer to the n -th entry of vector \mathbf{a} and the (m, n) -th entry of matrix \mathbf{A} , respectively. $\mathcal{O}(\cdot)$ denotes the order of complexity. $o(\cdot)$ denotes higher-order infinitesimals.

II. SYSTEM MODEL AND PERFORMANCE CHARACTERIZATION

A. Directivity Model of the Coupled MA Array

As illustrated in Fig. 1, we consider a linear MA array with N isotropic antenna elements located along the x -axis. The antenna position vector (APV) is denoted by

This work was supported in part by the National Key Research and Development Program of China under Grant 2025ZD1301900; in part by the Zhejiang Provincial Key Laboratory of Information Processing, Communication and Networking (IPCAN), Hangzhou, China. (Corresponding authors: Lipeng Zhu; Wenyan Ma.)

W. Xu and A. Liu are with the College of Information Science and Electronic Engineering, Zhejiang University, Hangzhou 310027, China (e-mails: 12231077@zju.edu.cn and anliu@zju.edu.cn).

Lipeng Zhu is with the State Key Laboratory of CNS/ATM and the School of Interdisciplinary Science, Beijing Institute of Technology, Beijing 100081, China (E-mail: zhulp@bit.edu.cn).

W. Ma, and R. Zhang are with the Department of Electrical and Computer Engineering, National University of Singapore, Singapore 117583 (e-mails: wenyan@u.nus.edu, elezhang@nus.edu.sg).

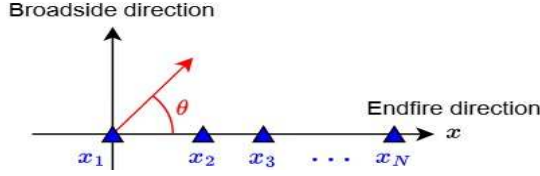


Fig. 1: Illustration of the considered linear MA array.

$\mathbf{x} = [x_1, x_2, \dots, x_N]^T \in \mathbb{R}^N$. We assume that the antennas can move on a line segment of length d_{\max} , and the minimum spacing between antennas is d_{\min} , i.e.,

$$d_{\min} \leq |x_m - x_n| \leq d_{\max}, \quad 1 \leq m \neq n \leq N. \quad (1)$$

The complex far-field pattern of the MA array over the direction $\theta \in [0^\circ, 180^\circ]$ is expressed as a function of $u \triangleq \cos \theta \in [-1, 1]$ for notation simplicity, where u is the direction cosine and is proportional to the discrete spatial frequency [4]:

$$y(u, \mathbf{x}) = \mathbf{w}^H \mathbf{a}(u, \mathbf{x}),$$

where $\mathbf{a}(u, \mathbf{x}) \in \mathbb{C}^{N \times 1}$ is the steering vector (SV):

$$\mathbf{a}(u, \mathbf{x}) = \left[e^{-j\frac{2\pi}{\lambda}x_1u}, e^{-j\frac{2\pi}{\lambda}x_2u}, \dots, e^{-j\frac{2\pi}{\lambda}x_Nu} \right]^T,$$

with λ denoting the wavelength. The vector $\mathbf{w} \in \mathbb{C}^{N \times 1}$ represents the coupled excitation coefficients, where the n -th entry w_n is proportional to the current excitation on the n -th antenna. Then, the total radiated power of the MA array is given by the integral in the angular domain [5]:

$$P_{\text{rad}} = \frac{1}{2} \int_0^\pi |\mathbf{a}^H(\cos \theta, \mathbf{x}) \mathbf{w}|^2 \sin(\theta) d\theta = \mathbf{w}^H \mathbf{R}(\mathbf{x}) \mathbf{w},$$

where we define

$$\mathbf{R}(\mathbf{x}) \triangleq \frac{1}{2} \int_0^\pi \mathbf{a}(u, \mathbf{x}) \mathbf{a}^H(u, \mathbf{x}) du,$$

which is also called impedance coupling matrix caused by power radiation interaction between antennas [5], [4], and the (m, n) -th entry of $\mathbf{R}(\mathbf{x})$ that represents the impedance coupling coefficient between the m -th antenna and the n -th antennas is $R_{mn}(\mathbf{x}) = \frac{1}{2} \int_{-1}^1 a_m(u, x_m) \overline{a_n(u, x_n)} du = \text{sinc}\left(2\frac{x_n - x_m}{\lambda}\right)$, with $\text{sinc}(x) = \frac{\sin(\pi x)}{\pi x}$.

Accordingly, the directivity of the MA array over the direction θ , expressed in terms of u , takes the form of a Rayleigh quotient $\mathring{G}_u(\mathbf{x}, \mathbf{w}) = \frac{|\mathbf{a}^H(u, \mathbf{x}) \mathbf{w}|^2}{\mathbf{w}^H \mathbf{R}(\mathbf{x}) \mathbf{w}}$. For a given \mathbf{x} , the optimal normalized \mathbf{w} for maximizing the directivity is given by $\mathbf{w}^* = \frac{\mathbf{R}^{-1}(\mathbf{x}) \mathbf{a}(u, \mathbf{x})}{\|\mathbf{R}^{-1}(\mathbf{x}) \mathbf{a}(u, \mathbf{x})\|_2}$, yielding the maximum directivity over u as a function of the APV:

$$G_u(\mathbf{x}) = \mathbf{a}^H(u, \mathbf{x}) \mathbf{R}^{-1}(\mathbf{x}) \mathbf{a}(u, \mathbf{x}). \quad (2)$$

In most existing works for MIMO system design, impedance coupling is neglected by constraining the inter-antenna spacing being greater than half-wavelength, since the sinc function becomes negligible for arguments larger than 1. Under this assumption, the radiated power, optimal beamforming vector, and maximum directivity simplify to $P_{\text{rad}} = \mathbf{w}^H \mathbf{w}$, $\mathbf{w}^* = \mathbf{a}(u, \mathbf{x}) / \sqrt{N}$, and $G_u = N$, respectively.

B. Directivity Gain Analysis

Direct analysis of the relationship between APV and directivity in (2) is challenging for a general array, primarily due to the presence of the inverse coupling matrix $\mathbf{R}^{-1}(\mathbf{x})$. To facilitate analysis, we interpret the coupling matrix $\mathbf{R}(\mathbf{x})$ as

the Gram matrix of the pattern functions $\{a_n(u, x_n)\}_{n=1}^N$ with the inner product defined as

$$\langle a_m(u, x_m), a_n(u, x_n) \rangle \triangleq \frac{1}{2} \int_{-1}^1 a_m(u, x_m) \overline{a_n(u, x_n)} du.$$

where $a_n(u, x_n) = e^{-j\frac{2\pi}{\lambda}x_nu}$ is the n -th entry of the SV $\mathbf{a}(u, \mathbf{x})$. To orthogonalize these pattern functions, we apply Cholesky decomposition denoted by $\mathbf{R}(\mathbf{x}) = \mathbf{L}(\mathbf{x}) \mathbf{L}^H(\mathbf{x})$. The inverse of the resulting lower-triangular matrix, $\mathbf{L}^{-1}(\mathbf{x})$, actually serves as the transformation matrix that explicitly constructs a set of orthonormal pattern functions (or effective SV) $\check{\mathbf{a}}(u, \mathbf{x}) = (\mathbf{L}(\mathbf{x}))^{-1} \mathbf{a}(u, \mathbf{x})$ via Gram-Schmidt process. This process proceeds orthonormalization recursively, with the n -th, $n = 1, 2, \dots, N$, pattern function $a_n(u, x_n)$ orthonormalized as:

$$\begin{aligned} \check{a}_n(u, x_n) &= a_n(u, x_n) \\ &- \sum_{m=1}^{n-1} \langle \check{a}_m(u, x_m), a_n(u, x_n) \rangle \check{a}_m(u, x_m), \end{aligned} \quad (3a)$$

$$\check{a}_n(u, x_n) = \frac{\check{a}_n(u, x_n)}{\sqrt{\langle \check{a}_n(u, x_n), \check{a}_n(u, x_n) \rangle}}. \quad (3b)$$

By defining the effective beamforming vector as $\check{\mathbf{w}} = \mathbf{L}^H(\mathbf{x}) \mathbf{w}$, the directivity simplifies to a canonical Rayleigh quotient form $\mathring{G}_u(\mathbf{x}, \mathbf{w}) = \frac{|\check{\mathbf{a}}^H(u, \mathbf{x}) \check{\mathbf{w}}|^2}{\check{\mathbf{w}}^H \check{\mathbf{w}}}$. The optimal effective beamforming vector is thus $\check{\mathbf{w}}^* = \frac{\check{\mathbf{a}}(u, \mathbf{x})}{\|\check{\mathbf{a}}(u, \mathbf{x})\|_2}$, and the corresponding maximum directivity is given by:

$$G_u(\mathbf{x}) = \|\check{\mathbf{a}}(u, \mathbf{x})\|_2^2 = \sum_{n=1}^N |\check{a}_n(u, x_n)|^2, \quad (4)$$

which are consistent with results in (2). This transformation incorporates the coupling matrix $\mathbf{R}(\mathbf{x})$ into the effective SV $\check{\mathbf{a}}(u, \mathbf{x})$, yielding a mathematical form identical to that of an uncoupled array. The key difference is that the elements in the effective SV, i.e., $\{\check{a}_n(u, x_n)\}_{n=1}^N$, are generally not unimodular, owing to the transformation by $(\mathbf{L}(\mathbf{x}))^{-1}$.

This formulation reveals a fundamental insight. For any given FPA array, the average directivity over the entire angular space is $\frac{1}{2} \int_{-1}^1 \sum_{n=1}^N |\check{a}_n(u, x_n)|^2 du$, which is always equal to N because the effective pattern functions are orthonormal, as defined in (3). In particular, for arrays with elements located at integer multiples of half-wavelength (including ULAH), we have $\mathbf{R}(\mathbf{x}) = \mathbf{I}_N$, $\check{\mathbf{a}}(u, \mathbf{x}) = \mathbf{a}(u, \mathbf{x})$, and thus the directivity remains a constant of $\sum_{n=1}^N |a_n(u, x_n)|^2 = N$ over all directions. In contrast, for MA arrays, the directivity over any direction can exceed N by leveraging the coupling effect via APV optimization, which is demonstrated by the following three examples.

1) *Example I:* We first consider a simple two-antenna case (i.e., $N = 2$). We set $x_1 = 0$ without loss of generality. Based on (3), the effective pattern functions are given by

$$\check{a}_1(u, 0) = 1, \quad \check{a}_2(u, x_2) = \frac{a_2(u, x_2) - \text{sinc}\left(\frac{2x_2}{\lambda}\right)}{\sqrt{1 - \text{sinc}^2\left(\frac{2x_2}{\lambda}\right)}}.$$

Then the directivity over any given u can be expressed as

$$G_u\left([0, x_2]^T\right) = 2 \frac{1 - \cos\left(2\pi \frac{x_2 u}{\lambda}\right) \text{sinc}\left(\frac{2x_2}{\lambda}\right)}{1 - \text{sinc}^2\left(\frac{2x_2}{\lambda}\right)}.$$

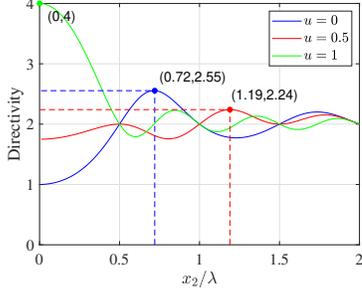


Fig. 2: Directivity versus $\frac{x_2}{\lambda}$ for $N = 2$ and $u = 0, 0.5, 1$.

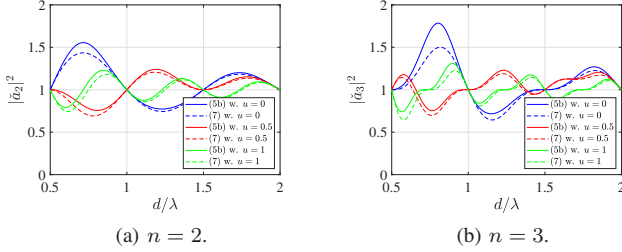


Fig. 3: For an ULA with $d > \frac{\lambda}{2}$, approximation of $|\tilde{a}_n(u, x_n)|^2$ via (5) against squared magnitude of (3b) versus d for $n = 2, 3$ and $u = 0, 0.5, 1$.

Over the broadside direction (i.e., $u = 0$), this simplifies to $G_u = \frac{2}{1 + \text{sinc}(2\frac{x_2}{\lambda})}$. The optimal position $x_2 \approx 0.72\lambda$ yields a maximum directivity of $G_u^* \approx 2.55$. Over the endfire direction (i.e., $u = 1$), $x_2 \rightarrow 0$ yields superdirectivity $G_u \rightarrow 4$. Both cases achieve a directivity larger than the number of antennas ($N = 2$). However, over other directions, the optimal solution for x_2 becomes analytically complicated. The relationship between directivity of the two-antenna MA array and x_2 is depicted in Fig. 2.

2) *Example II*: For an array with inter-antenna spacing greater than half-wavelength, i.e., $|x_m - x_n| > \frac{\lambda}{2}, \forall m \neq n$, the coupling effects are weak. For convenience, we define $k_{mn} = \frac{2\pi(x_m - x_n)}{\lambda}, \forall m \neq n$, and the magnitude of coupling coefficient $|\text{sinc}(\frac{k_{mn}}{\pi})| < 0.22$ since $\frac{k_{mn}}{\pi} > 1$. By neglecting higher-order terms $o(\text{sinc}(\frac{k_{mn}}{\pi}))$, $\forall m \neq n$, the orthogonalization in (3) can be simplified as follows:

$$\tilde{a}_1(u, 0) \equiv 1, \tilde{a}_2(u, x_2) \approx -\text{sinc}\left(\frac{k_{12}}{\pi}\right) + a_2(u, x_2), \dots,$$

$$\tilde{a}_N(u, x_N) \approx -\sum_{n=1}^{N-1} \text{sinc}\left(\frac{k_{nN}}{\pi}\right) e^{-jk_{nN}u} + a_N(u, x_N).$$

Under this first-order approximation, the squared magnitude of each orthogonalized pattern simplifies to

$$|\tilde{a}_n(u, x_n)|^2 \approx 1 - 2 \sum_{m=1}^{n-1} \text{sinc}\left(\frac{k_{mn}}{\pi}\right) \cos(k_{mn}u). \quad (5)$$

To validate this approximation, we consider an ULA with element spacing $d > \frac{\lambda}{2}$, i.e., $x_n = (n-1)d$. The behavior of the approximated $|\tilde{a}_n(u, (n-1)d)|^2$ in (5) as a function of $\frac{d}{\lambda}$ is illustrated in Fig. 3.

Consequently, the overall directivity $G_u(\mathbf{x})$ is given by

$$\sum_{n=1}^N |\tilde{a}_n(u, x_n)|^2 \approx N - 2 \sum_{1 \leq m < n \leq N} \text{sinc}\left(\frac{k_{mn}}{\pi}\right) \cos(k_{mn}u).$$

A special case arises for the broadside direction ($u = 0$). In this case, maximizing the directivity is equivalent to minimizing the sum $\sum_{1 \leq m < n \leq N} \text{sinc}\left(\frac{k_{mn}}{\pi}\right)$. If only mutual coupling between adjacent elements is considered, the directivity can be further simplified as $G_u(\mathbf{x}) \approx N - 2 \sum_{n=2}^N \text{sinc}\left(2\frac{x_n - x_{n-1}}{\lambda}\right)$. Under this simplified model, the optimal APV reduces to an ULA with $d \approx 0.72\lambda$, yielding a directivity of

$$G_u(\mathbf{x}) \approx 1.44N - 0.44. \quad (6)$$

The directivities over the broadside direction for ULAs with $d \approx 0.72\lambda$ under different values of N are shown in Table I.

N	2	3	4	5
Directivity in (4)	2.55	4.13	5.49	6.88
Approximation in (6)	2.44	3.88	5.32	6.76

TABLE I: Approximated directivity in (6) against actual directivity in (4) under different values of N .

For arrays with elements $N \geq 3$, the directivity over the broadside direction can be further enhanced by fine-tuning antenna positions to exploit mutual coupling effects from non-adjacent elements.

3) *Example III*: For a superdirective array, i.e., $x_n = (n-1)d$ with $d \rightarrow 0$, we define $k = \frac{2\pi d}{\lambda} \rightarrow 0$ for convenience, and the pattern functions orthogonalized via (3a) are given by

$$\tilde{a}_1(u, 0) \equiv 1, \tilde{a}_2(u, d) = -jku + o(k),$$

$$\tilde{a}_3(u, 2d) = \frac{2}{3}k^2 + 2k^2u^2 + o(k^2), \dots,$$

where higher-order terms $o(k^{n-1})$ in $\tilde{a}_n(u, (n-1)d)$ can be neglected. After normalization, the effective pattern functions correspond to $\check{a}_n(u, (n-1)d) = \sqrt{2n-1}P_{n-1}(u)$, $n = 1, 2, \dots, N$, where $P_n(\cdot)$ is the n -th order Legendre polynomial [14] with $P_0(u) = 1$, $P_1(u) = u$, $P_2(u) = \frac{3u^2-1}{2}$, etc. The directivity thus becomes $\sum_{n=1}^N (2n-1) |P_{n-1}(u)|^2$, which attains a maximum of N^2 over the endfire direction ($u = \pm 1$).

For a general N -antenna MA array, a closed-form solution for the optimal APV is intractable. In the following, we aim to optimize the APV numerically. The optimization problem can be formulated as follows:

$$\max_{x_2, x_3, \dots, x_N} G_u(\mathbf{x}) \quad (7a)$$

$$\text{s.t.} \quad (1). \quad (7b)$$

III. PROPOSED ALGORITHM

Since $x_1 = 0$, the rest $(N-1)$ antennas are constrained within the movable region $\mathcal{P} = [-d_{\max}, -d_{\min}] \cup [d_{\min}, d_{\max}]$, while simultaneously satisfying the constraints specified in (7b). We propose a computationally efficient two-stage algorithm for optimizing x_2, \dots, x_N . In the first stage, the $(N-1)$ antenna positions are selected from grid points sampled over \mathcal{P} based on greedy search (GS). In the second stage, the antenna positions are refined continuously based on GD.

A. Grid Points Selection Based on GS

We sample M grid points $\tilde{\mathcal{X}} \triangleq \{\tilde{x}_1, \tilde{x}_2, \dots, \tilde{x}_M\}$ with uniform spacing d_g ($d_g < d_{\min}$) over \mathcal{P} . We define an index vector $\mathcal{M} \triangleq [\mathcal{M}_2, \mathcal{M}_3, \dots, \mathcal{M}_N]^T$, where each $\mathcal{M}_n \in$

$\{1, 2, \dots, M\}$ corresponds to the grid point index for the n -th antenna position.

The GS procedure optimizes these indexes sequentially. In the n -th step ($n = 1, 2, \dots, N - 1$), the positions of the first n antennas are fixed. The algorithm then selects the optimal grid point for x_{n+1} by exhaustively evaluating all candidate points in $\tilde{\mathcal{X}}$ that satisfy the position constraints in (7b), with the goal of maximizing the directivity of the $(n + 1)$ -element array. The GS sub-problem in the n -th step is thus given by

$$\max_{\mathcal{M}_{n+1}} G_u \left([0, x_2^{GS}, \dots, x_n^{GS}, \tilde{x}_{\mathcal{M}_{n+1}}]^T \right) \quad (8a)$$

$$\text{s.t. } d_{\min} \leq |\tilde{x}_{\mathcal{M}_{n+1}} - x_n^{GS}| \leq d_{\max}, 2 \leq m \leq n, \quad (8b)$$

which can be efficiently solved by the one-dimension (1D) exhaustive search (ES), with the optimal solution denoted as \mathcal{M}_{n+1}^* . The selected position is fixed as $x_{n+1}^{GS} = \tilde{x}_{\mathcal{M}_{n+1}^*}$ for subsequent steps.

B. Antenna Positions Refinement Based on GD

Since the optimal positions generally do not lie exactly on the discrete grid points in $\tilde{\mathcal{X}}$, we employ GD for continuous refinement. Specifically, we denote the maximum iteration number and the APV obtained in the t -th iteration as T and $\mathbf{x}(t)$, respectively. The APV is initialized as the output of the GS process denoted as $\mathbf{x}^{GS} = [0, x_2^{GS}, \dots, x_N^{GS}]^T$, i.e., $\mathbf{x}(0) = \mathbf{x}^{GS}$. Then, the t -th iteration is detailed as follows.

First, by defining $\hat{\mathbf{a}}(t) = \mathbf{R}^{-1}(\mathbf{x}(t)) \mathbf{a}(u, \mathbf{x}(t))$, the partial derivatives of the objective function $G_u(\mathbf{x})$ with respect to (w.r.t.) $x_n, n = 2, \dots, N$ are given by

$$\frac{\partial G_u(\mathbf{x})}{\partial x_n} = 2\Re \left(\hat{\mathbf{a}}^H(t) \frac{\partial \mathbf{a}(u, \mathbf{x})}{\partial x_n} \right) - \hat{\mathbf{a}}^H(t) \frac{\partial \mathbf{R}(\mathbf{x})}{\partial x_n} \hat{\mathbf{a}}(t), \quad (9)$$

where elements in $\frac{\partial \mathbf{a}(u, \mathbf{x})}{\partial x_n} \in \mathbb{R}^N$ are all zeros except the n -th element $\left(\frac{\partial \mathbf{a}(u, \mathbf{x})}{\partial x_n} \right)_n = -j \frac{2\pi}{\lambda} u e^{-j \frac{2\pi}{\lambda} x_n(t) u}$, and elements in $\frac{\partial \mathbf{R}(\mathbf{x})}{\partial x_n} \in \mathbb{R}^{N \times N}$ are all zeros except elements in the n -th row and elements in the n -th column $\left(\frac{\partial \mathbf{R}(\mathbf{x})}{\partial x_n} \right)_{mn} = \begin{cases} 0, & m = n, \\ \frac{\cos(\pi(x_n(t) - x_m(t))) - \text{sinc}(x_n(t) - x_m(t))}{x_n(t) - x_m(t)}, & m \neq n. \end{cases}$

Next, the APV is updated using an adaptive step size α , initialized as α_0 . A candidate update for $\mathbf{x}(t)$ is computed as

$$\mathbf{x}^{test} = \mathbf{x}(t) + \alpha \left[0, \frac{\partial G_u}{\partial x_2}, \dots, \frac{\partial G_u}{\partial x_N} \right]^T. \quad (10)$$

This candidate is accepted only if it satisfies two conditions: On one hand, it improves the objective function, i.e., $G_u(\mathbf{x}^{test}) > G_u(\mathbf{x}(t))$; on the other hand, it satisfies the position constraints in (7b). Otherwise, α is halved in a backtracking line search until the conditions are satisfied or α is below the threshold ϵ .

C. Algorithm Summary

The proposed algorithm is summarized in Algorithm 1. Lines 1-4 correspond to the GS stage, while lines 5-16 correspond to the GD stage. The convergence of GD is guaranteed because the objective function is upper-bounded, and non-decreasing in iterations. The computational complexity is analyzed as follows. The directivity evaluation in (4) of M candidate grid points for \mathcal{M}_{n+1} in line 3 can be reduced

Algorithm 1 GS-GD for Antenna Position Optimization

Input: $N, \theta, \lambda, d_{\max}, d_{\min}, d_g, \alpha_0, \epsilon$.

- 1: %% The first stage: GS to select the antenna positions from grid points.
- 2: **for** $n = 1 \dots N - 1$ **do**
- 3: Optimize \mathcal{M}_{n+1} by solving (8).
- 4: **end for**
- 5: %% The second stage: GD to continuously refine the positions via backtracking line search.
- 6: Initialize $\mathbf{x}(0) = \mathbf{x}^{GS}$.
- 7: **for** $t = 0 \dots T - 1$ **do**
- 8: Compute the gradients $\frac{\partial G_u(\mathbf{x})}{\partial x_n}, n = 2, \dots, N$ as (9).
- 9: Initialize $\alpha = \alpha_0, r = -1, \mathbf{x}^{test} = \mathbf{x}(t)$.
- 10: **while** $r < 0$ or \mathbf{x}^{test} does not satisfy (7b) **do**
- 11: Update \mathbf{x}^{test} as (10).
- 12: Compute $r = G_u(\mathbf{x}^{test}) - G_u(\mathbf{x}(t))$.
- 13: $\alpha \leftarrow 0.5\alpha$.
- 14: **if** $\alpha < \epsilon$ **then**
- 15: Return $\mathbf{x}^* = \mathbf{x}(t)$.
- 16: **end if**
- 17: **end while**
- 18: Update $\mathbf{x}(t + 1) = \mathbf{x}^{test}$.
- 19: **end for**
- 20: $\mathbf{x}^* = \mathbf{x}(T)$.

Output: \mathbf{x}^* .

Parameter	Value
Number of antennas N	5
Wavelength λ	0.3 m
Minimum spacing d_{\min}	$\lambda/10 = 0.03$ m
Aperture size d_{\max}	$\frac{N-1}{2}\lambda, (N-1)\lambda, 2(N-1)\lambda$
Grid spacing d_g	$\lambda/20 = 0.015$ m
GS-GD iterations T	5
Initial step size α_0	1
Tolerance ϵ	10^{-3}

TABLE II: Main simulation parameters.

to computing $\{\tilde{a}_{n+1}(u, x)\}_{x \in \tilde{\mathcal{X}}}$ with complexity $\mathcal{O}(Mn^2)$, since $\{\tilde{a}_m(u, x_m^{GS})\}_{m=1}^n$ are recursively computed in former steps. The complexity of calculating the gradients in line 8 is $\mathcal{O}(N^2)$. The complexity of calculating the objective function in line 12 is $\mathcal{O}(N^3)$, and thus the maximum complexity of the entire while loop is $\mathcal{O}(\log_2(\frac{\alpha_0}{\epsilon}) N^3)$. Hence, the overall computational complexity of the proposed Algorithm 1 is $\mathcal{O}(MN^3 + T(N^2 + \log_2(\frac{\alpha_0}{\epsilon}) N^3))$.

IV. NUMERICAL RESULTS

This section presents numerical results to validate the directivity enhancement of the MA array by taking into the antenna coupling effect and the performance of the proposed GS-GD algorithm. For clarity, the directivity is presented as a function of the angle θ rather than u in this section. Furthermore, the results are confined to $\theta \in [0^\circ, 90^\circ]$, as the directivity is symmetric w.r.t. 90° . The main simulation parameters are summarized in Table II for ease of reference.

First, we compare the directivity of the optimized coupled MA array with the traditional ULAH. In simulations, we employ an ES over all discretized grid points to approximate the globally optimal solution for problem (7). The results are shown in Fig. 4.

The results demonstrate that, over all directions, the optimized MA array achieves a higher directivity compared to the

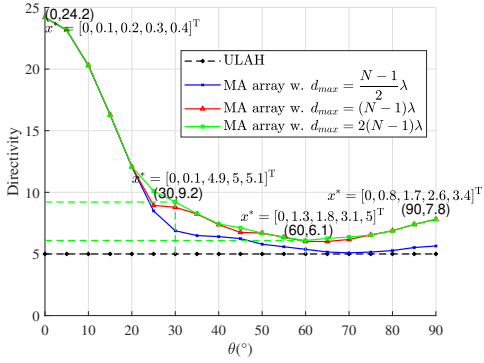


Fig. 4: Directivity of the coupled MA array compared to the ULAH in different values of θ and d_{\max} .

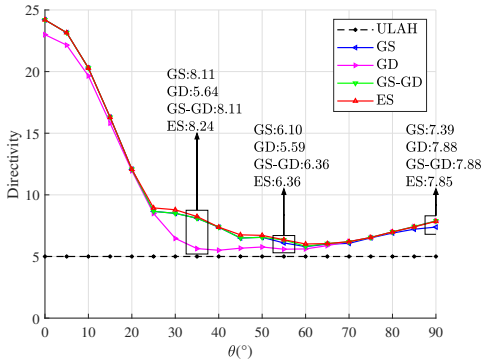


Fig. 5: Comparison of the proposed GS-GD algorithm with baselines in different values of θ .

ULAH. Specifically, when $\theta \rightarrow 0^\circ$, the superdirective array is optimal, and the directivity approaches N^2 . As θ increases, the optimal antenna positions exhibit irregular patterns, and there is at least 20% improvement in the directivity for the coupled MA array compared to the traditional ULAH without antenna coupling when the movable region is sufficiently large. When $\theta \rightarrow 90^\circ$, the optimal array converges to a nearly uniform array with spacing around 0.8λ , and there is around 50% directivity gain, which are consistent with the analysis in Section II-B2. Additionally, over the vast majority of directions, the maximum directivity for $d_{\max} = (N-1)\lambda$ is the same as that for $d_{\max} = 2(N-1)\lambda$, both of which substantially exceed the directivity for $d_{\max} = \frac{1}{2}(N-1)\lambda$, which implies that $d_{\max} = (N-1)\lambda$ is sufficient to achieve most of the directivity gains in practice.

Next, we evaluate the performance of the proposed GS-GD algorithm against the following baseline methods:

- ES: This method selects antenna positions from grid points, and compute the directivity of all feasible APV cases to find the maximum directivity.
- GS: This method only performs the first stage as mentioned in Section III-A.
- GD: This method initializes the APV as a ULAH, and then performs the second stage as mentioned in Section III-B, where we set $T = 30$ in simulations to ensure convergence.
- ULAH: For ULAH without antenna coupling, the directivity is N over all directions.

The performance of the algorithms is evaluated in Fig. 5. As shown in the figure, the performance of the proposed

GS-GD approaches ES over most directions. Moreover, GS-GD outperforms the two baselines (GS and GD) over all directions. This superiority arises from its ability to mitigate the inherent limitations of both methods: GS is constrained by its sequential optimization process, which myopically adjusts individual antenna positions, thus lacking the capability to co-optimize the entire array, while GD is prone to local optima when initialized from a ULAH. By leveraging both approaches, GS-GD enables a more robust search, consistently converging to a solution closer to the global optimum.

V. CONCLUSION

In this paper, we investigated the directivity of MA arrays with antenna coupling. In contrast to traditional uncoupled arrays, coupled MA arrays can enhance the directivity (i.e., beamforming gain) by concentrating the radiated power more effectively toward specific directions. We aimed to optimize the positions of antennas for maximizing the directivity of the MA array over any given direction. A low-complexity GS-GD algorithm was proposed, where the antenna positions are first selected sequentially from discrete grid points through GS and then continuously refined through GD optimization. Numerical results demonstrated the directivity gain of the optimized coupled MA array and the efficiency of the proposed GS-GD algorithm.

REFERENCES

- [1] J. G. I. Singh, and D. K. Choudhary, "Gain and isolation improvement techniques for MIMO antenna: A compendious survey," *Results in Engineering*, vol. 25, p. 104482, Mar. 2025.
- [2] T. T. Vo, L. Ouvry, A. Sibille, and S. Bories, "Mutual coupling modeling and calibration in antenna arrays for AOA estimation," in *2018 2nd URSI Atl. Radio Sci. Meet. -RASC*. Gran Canaria: IEEE, May 2018, pp. 1–4.
- [3] T. L. Marzetta, "Super-directive antenna arrays: Fundamentals and new perspectives," in *2019 53rd Asilomar Conf. Signals Syst. Comput.* Pacific Grove, CA, USA: IEEE, Nov. 2019, pp. 1–4.
- [4] A. Pizzo and A. Lozano, "Superdirectivity in linear holographic MIMO," in *2024 IEEE 25th Int. Workshop Signal Process. Adv. Wirel. Commun. SPAWC*. Lucca, Italy: IEEE, Sep. 2024, pp. 386–390.
- [5] L. Han, H. Yin, M. Gao, and J. Xie, "A superdirective beamforming approach with impedance coupling and field coupling for compact antenna arrays," *IEEE Open J. Commun. Soc.*, vol. 5, pp. 7262–7277, 2024.
- [6] L. Zhu, W. Ma, and R. Zhang, "Modeling and performance analysis for movable antenna enabled wireless communications," *IEEE Trans. Wirel. Commun.*, vol. 23, no. 6, pp. 6234–6250, Jun. 2024.
- [7] —, "Movable antennas for wireless communication: Opportunities and challenges," *IEEE Commun. Mag.*, vol. 62, no. 6, pp. 114–120, Jun. 2024.
- [8] W. Ma, L. Zhu, and R. Zhang, "Compressed sensing based channel estimation for movable antenna communications," *IEEE Commun. Lett.*, vol. 27, no. 10, pp. 2747–2751, Oct. 2023.
- [9] X. Shao, Q. Jiang, and R. Zhang, "6D movable antenna based on user distribution: Modeling and optimization," *IEEE Trans. Wirel. Commun.*, vol. 24, no. 1, pp. 355–370, Jan. 2025.
- [10] X. Shao, R. Zhang, Q. Jiang, and R. Schober, "6D movable antenna enhanced wireless network via discrete position and rotation optimization," *IEEE J. Sel. Areas Commun.*, vol. 43, no. 3, pp. 674–687, Mar. 2025.
- [11] L. Zhu, W. Ma, and R. Zhang, "Movable-antenna array enhanced beamforming: Achieving full array gain with null steering," *IEEE Commun. Lett.*, vol. 27, no. 12, pp. 3340–3344, Dec. 2023.
- [12] P. Mursia, F. Devoti, M. Rossanese, V. Sciancalepore, G. Gradoni, M. D. Renzo, and X. Costa-Pérez, "T3dris: Advancing conformal ris design through in-depth analysis of mutual coupling effects," *IEEE Trans. Commun.*, vol. 73, no. 2, pp. 889–903, Feb. 2025.
- [13] J. Zhu, F. Han, Y. Guo, and Y. Wang, "Mutual coupling-enhanced movable antenna arrays: Breaking minimum-spacing constraints," *IEEE Commun. Lett.*, vol. 30, pp. 672–676, 2026.
- [14] D. Y. Levin, S. Markovich-Golan, and S. Gannot, "Near-field superdirectivity: An analytical perspective," *IEEE/ACM Trans. Audio Speech Lang. Process.*, vol. 29, pp. 1661–1674, 2021.